An alternative methodology in Schottky diode physics

J. Mitra, L. Feng, L. Peñate-Quesada, and P. Dawson

An alternative methodology in Schottky diode physics

J. Mitra,[1,a)] L. Feng,[2] L. Peñate-Quesada,[3] and P. Dawson[2]

[1]*School of Physics, Indian Institute of Science Education and Research, Thiruvananthapuram 695016, India*
[2]*Centre for Nanostructured Media, School of Mathematics and Physics, Queen's University, Belfast BT7 1NN, United Kingdom*
[3]*ALTER Technology Group, 28760 Tres Cantos, Madrid, Spain*

The fabrication and electrical characterization of Schottky junction diodes have been extensively researched for three-quarters of a century since the original work of Schottky in 1938. This study breaks from the highly standardized regime of such research and provides an alternative methodology that prompts novel, more efficient applications of the adroit Schottky junction in areas such as chemical and thermal sensing. The core departure from standard Schottky diode configuration is that the metal electrode is of comparable or higher resistance than the underlying semiconductor. Further, complete electrical characterization is accomplished through recording four-probe resistance-temperature (R_D-T) characteristics of the device, where electrical sourcing and sensing is done only via the metal electrode and not directly through the semiconductor. Importantly, this results in probing a nominally unbiased junction while eliminating the need for an Ohmic contact to the semiconductor. The characteristic R_D-T plot shows two distinct regions of high (metal) and low (semiconductor) resistances at low and high temperatures, respectively, connected by a crossover region of width, ΔT, within which there is a large negative temperature coefficient of resistance. The R_D-T characteristic is highly sensitive to the Schottky barrier height; consequently, at a fixed temperature, R_D responds appreciably to small changes in barrier height such as that induced by absorption of a chemical species (e.g., H_2) at the interface. A theoretical model is developed to simulate the R_D-T data and applied to Pd/p-Si and Pt/p-Si Schottky diodes with a range of metal electrode resistance. The analysis gives near-perfect fits to the experimental R_D-T characteristics, yielding the junction properties as fit parameters. The modelling not only helps elucidate the underlying physics but also helps to comprehend the parameter space essential for the discussed applications. Although the primary regime of application is limited to a relatively narrow range (ΔT) for a given type of diode, the alternative methodology is of universal applicability to all metal-semiconductor combinations forming Schottky contacts. © 2015 AIP Publishing LLC.
[http://dx.doi.org/10.1063/1.4922974]

I. INTRODUCTION

The pioneering work of Schottky[1] and Mott[2] on the potential barrier formed at a metal/semiconductor interface dates back to 1938. Later, Bethe[3] developed the concept of thermionic emission to describe the flow of current across the barrier. Since these foundational works, the Schottky diode has become deeply embedded and extensively deployed in the semiconductor industry and till today attracts a great deal of research interest. Key properties are a very low reverse bias leakage current and a fast response time, and these underpin some more recent developments such as Schottky diode-based components for THz communications (e.g., sources,[4] sensors,[5] and modulators[6]) and the Schottky-barrier MOSFET,[7–9] which displays a significantly higher (up to 10^4) on-to-off current ratio relative to its conventional counterpart with doped-semiconductor source and drain. In recent years, much electronic device research has been materials driven and, in the context of the Schottky diode, the emphasis lies decidedly on the semiconductor side of the

barrier. Investigations have addressed the formation and characteristics of Schottky contacts on SiC,[10] GaN,[11] and ZnO[12,13] substrates, for example. In the realm of nanostructured media, Schottky contacts have been formed with GaN nanowires,[14] ZnO nanorods,[15] InP nanoneedles,[16] and semiconducting carbon nanotubes.[17,18]

The Schottky barrier (SB) interface itself has been the focus of much experimentation with the electrical properties frequently characterized in terms of plots of current against voltage (as a function of temperature), I-V(-T), and capacitance versus voltage, C-V. The SB height is a primary characterization parameter and its modification for a given metal/semiconductor combination has been studied as a function of the semiconductor surface treatment prior to metal deposition,[19] delta-doping at the semiconductor surface,[20] the method of metal deposition,[21] the presence of molecular species at the Schottky interface,[22,23] and even post-fabrication ion implanting and drive-in annealing.[24] The influence of molecular species on the SB height is, of course, the basis for gas sensing[25,26] using Schottky diodes, in particular, hydrogen sensing.[27–30] Previously, we have reported ultrahigh-sensitivity hydrogen detection employing the methodology developed here with Pd as the metal electrode.[31]

a)Author to whom correspondence should be addressed. Electronic mail: j.mitra@iisertvm.ac.in

Complementing the experimental work, there have been numerous theoretical and modeling studies aimed at understanding SB characteristics. As regards the SB height, one of the more salient features has been the development of analysis incorporating non-homogeneous barrier heights,[32–36] giving a physical basis to the ideality factor that is introduced in an empirical manner within the application of the thermionic emission model to I-V-T data. A detailed review of the physics and chemistry of Schottky barrier formation and characteristics has been given recently by Tung.[37]

By contrast, the metal side of the barrier per se is visited less frequently. Beyond the use of metals and metal silicides, there has been some investigation where the "metal" electrode is a material of a more topical nature such as graphite[38] or graphene,[39–44] or where it has comprised a nanoparticulate layer[29] or indeed even a metallic metamaterial.[6] The work reported here is distinctive in that it focuses on the metal side of the barrier, specifically the use of resistive metal electrodes, but in combination with electrical measurements where the contacts are made to the metal electrode only (Figure 1). While the measurement of device resistance obtained as a function of temperature (R_D-T) is ostensibly just that of the metal electrode, the underlying semiconductor and SB in fact play a critical, temperature-dependent role, such that the R_D-T measurement can constitute a simple, single-run method of characterizing the Schottky junction properties along with their temperature dependence. This may be regarded as complementary or alternative to the usual multi-run I-V-T method. Such characterization requires quantitative modeling of the R_D-T data where properties of the semiconductor, SB and metal act as input parameters as reported here. The core feature that the experiment yields, and that any model must describe, is a region of negative temperature coefficient of resistance (NTR) in the R_D-T plots (Figures 2 and 3).

In stating that the metal electrode is resistive, this is relative to a portion of the underlying semiconductor of similar

FIG. 2. Semi-log plot of resistance vs. temperature for a series of Pd/p-Si devices of length $L = 160 \, \mu m$ and widths $w = 16$, 32, and $64 \, \mu m$, as indicated in the figure. The experimental data (R_D) are plotted as open circles and the solid lines are a fit to the data, generated by the model (see text).

lateral dimensions. Since any metal can be made thin enough to be resistive, the methodology discussed here is not restrictive; thus, common metals (and metal silicides) used in Schottky diode formation are perfectly adequate to illustrate the main points, as is the use of Si and industry-standard III–V semiconductor substrates, rather than anything more topical or esoteric. Here, results from Pt/p-Si and Pd/p-Si devices are analyzed in detail, while we have reported a less in-depth survey of a broader range of Schottky contacts using this methodology elsewhere.[45] In the results discussed below, the metal electrode resistance lies in the range of 0.2–40 kΩ.

The Schottky configuration discussed here represents something of a blind spot in the field. This obviously prompts the question of why should there be such a gap in the field the first place? We suggest that this is due to two factors individually and in combination: (a) metal electrodes in Schottky devices are nearly always much thicker (∼100 nm or greater) and thus non-resistive in the terms discussed here, and (b) electrical measurements are nearly always conducted directly across the device with contact electrodes on opposite sides of the SB in order to avail of the rectifying properties. Thus, even when the use of ultra-thin
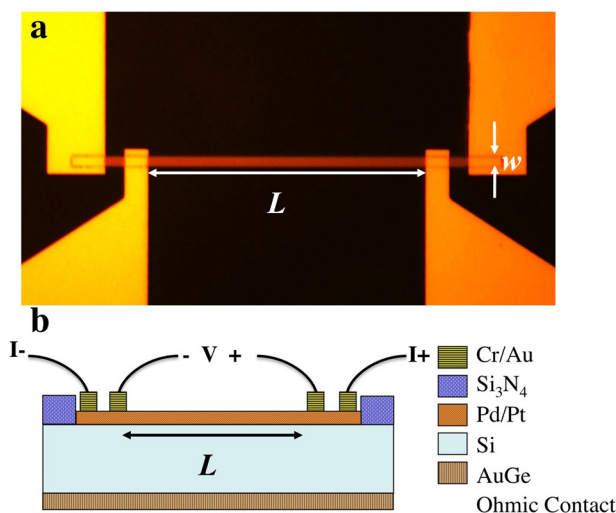

FIG. 1. (a) Optical micrograph of a Schottky device showing a thin, high aspect ratio Pt electrode of length, L (between the innermost pair of a set of four Cr/Au contact electrodes) and width w. (b) Schematic of the Schottky device cross section.
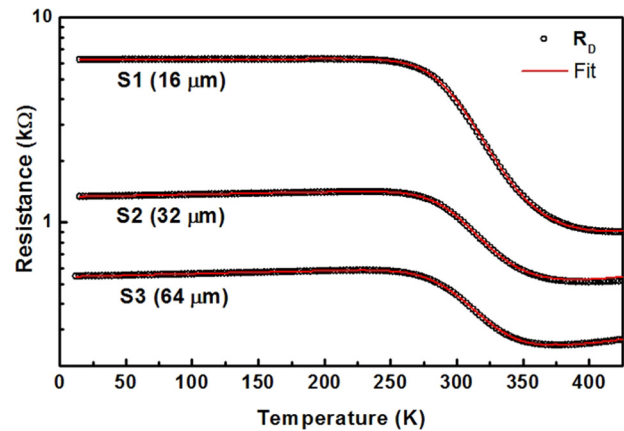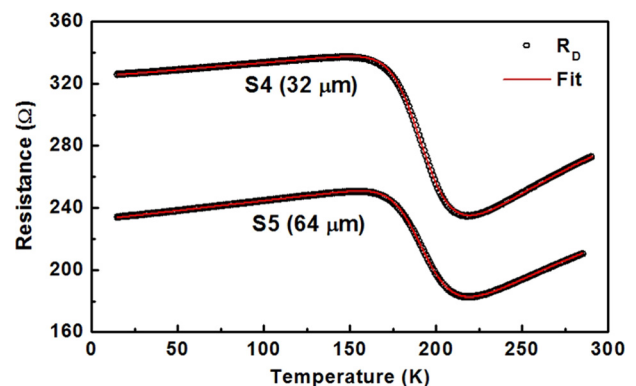

FIG. 3. Semi-log plot of resistance vs. temperature for a set of two Pt/p-Si devices of length $L = 160 \, \mu m$ and widths $w = 32$ and $64 \, \mu m$, as indicated in the figure. The experimental data (R_D) are plotted as open circles and the solid lines are a fit to the data, generated by the model (see text).

metallic electrodes has been routine technology in specific contexts in the past, notably, for example, in PtSi/p-Si array detectors,[46,47] where the PtSi electrode is typically 2–5 nm thick (i.e., even when statement (a) does not apply), the implementation of (b) means that the NTR effect addressed here is not routinely observed. On the other hand, the key result of NTR in the R_D-T plot is not entirely unknown in the literature, but has featured only very rarely so far as we are aware.[48,49] Overall, the present scheme (R_D-T measurement) of characterizing a Schottky junction across a wide temperature range has not been methodically investigated experimentally nor has it been quantitatively analyzed or modelled. We address these issues here, highlighting the distinctive advantages this technique offers and how it can lead to more efficacious application of Schottky devices in established and newer areas.

II. EXPERIMENT

The Pd/p-Si and Pt/p–Si Schottky devices were fabricated on p-type (boron doped), 500 μm thick Si (100) wafers of resistivity 1–10 Ω cm ($N_A > 1 \times 10^{15}$ cm^{-3}). Figure 1 shows an optical micrograph (top-view) of the device, the inset sketching the cross-section. Prior to device fabrication, standard cleaning procedures were followed to remove any organic residues. The native oxide was removed using buffered HF (HF:H$_2$O = 1:10) solution; this was followed by the controlled growth of a thicker ($\sim$80 nm), high quality oxide layer in which the device window was etched. The Schottky interface was then formed by electron beam evaporation of a thin Pd or Pt strip of width, w, length L, and thickness, $t \lesssim 10$ nm, onto the clean, exposed Si surface, defined by the window in the overlying oxide layer. Lift-off was used to remove the metal over the remainder of the wafer. In a second lithography step, the thin metal electrode was contacted with four metal contact pads (as illustrated in Figure 1), which were used for measuring the four-probe device resistance R_D. In addition, an Ohmic back contact was formed in order to facilitate conventional cross-barrier I–V measurements. The device patterning, using standard optical lithography techniques, was performed at the Phillips Mi-Plaza facility, Eindhoven, The Netherlands.

The linear four-probe resistance R_D-T measurements (along the metal electrodes) were carried out in the temperature interval of 15–425 K in a CTI Cryotronics closed cycle He refrigerator system, operating at a base pressure of $\sim$10^{-6} mbar and equipped with a temperature controller (Lakeshore 22C). The current-voltage (I-V) characteristics (across the Schottky barrier) were measured at various temperatures (temperature stability <500 mK), using a programmable source meter (HP4000A). While conducting the R_D-T measurements, no electrical contacts were directly made to the semiconductor.

In this study, we have investigated electrical transport along a range of these elongated Schottky diodes in which the metal electrode is varied systematically in width (16, 32, and 64 μm), while the length, L, is kept constant at 160 μm. We present data from a selected number of samples, S1-S5, as specified in Table I.

III. RESULTS AND PHYSICAL EXPLANATION

The R_D-T results of Figures 2 and 3 were obtained utilising samples of the type illustrated in Figure 1. Figure 2 shows a semilog R_D-T plot for a set of Pd/p-Si samples (S1–S3) from 15 to 425 K. For all plots, the device resistance, R_D, exhibits a linear section at low temperatures, reaches a maximum (R_{max}) at a temperature $T_1 \sim 250$ K, above which it falls sharply, i.e., exhibits a negative temperature coefficient (dR_D/d$T < 0$), before reaching a minimum resistance R_{min} at $T_2 \sim 350$–400 K. A similar temperature dependence of R_D is observed for the Pt/p-Si samples, S4 and S5 (Figure 3). Above T_2, dR_D/dT can be seen to change sign again and is, in general, non-linear in nature. Thus, as a function of temperature, the R_D-T plots exhibit a metal–insulator–metal transition, as denoted by the sign of dR_D/dT of the curves. We define the transition as being of magnitude $\Delta R_D = R_{max}$–R_{min}, and occurring at temperature $T_C = (T_1 + T_2)/2$ with a width $\Delta T = (T_2$–$T_1)$. The values of T_C, ΔT, and ΔR_D are tabulated in Table I for each of the samples S1–S5, along with the type and width of the metal electrode and doping density of the semiconductor substrate. T_C is seen to be relatively independent of the geometric properties (sample width) for both Pd and Pt samples. ΔT and ΔR_D both increase with decreasing sample width, showing that the transition takes place over a wider temperature range for narrower samples. However, their ratio $\Delta R_D/\Delta T$ indicates that the transition becomes progressively sharper, in terms of absolute gradient, with decreasing width (see Table I). Thus, the slope of the transition can be determined by controlling the width (resistance) of the metal layer alone.

In performing these measurements, the outermost contacts to the thin metal (Pd or Pt) electrode act as the source and drain of electric current (denoted as $I+$ and $I-$ in Figure 1(b)). The potential developed between the inner two electrodes is measured to obtain R_D. Importantly, no external bias is explicitly applied across the SB. However, even in the absence of a direct bias, any carrier injected into the Pd or Pt strip can be excited across the SB into the semiconductor and so is not necessarily confined to the metal alone. This is the key issue in the device set-up here and it is now tracked from low to high temperature.

Starting from $T \ll T_1$, the probability of thermionic emission over the SB is negligible, resulting in confinement of the carriers to the resistive metal electrode. In this regime, electrical transport takes place only through the metal, evidenced by the positive, linear dependence of R_D on temperature. The most interesting behaviour of the device resistance occurs in the region of $T \sim T_C$. The collapse in resistance for $T > T_1$ is a direct consequence of an increase in thermal excitation of carriers across the SB, bringing the semiconductor into play as a parallel, current carrying channel. This process continues until R_D reaches R_{min} at T_2 where further increase in the thermally driven barrier crossing is no longer effective in reducing the overall device resistance—the region of NTR comes to an end. At higher temperatures, in the regime $T > T_2$, carriers cross the SB with ease, and the resistance of the semiconductor substrate determines R_D predominantly, whereupon a positive (variable) temperature coefficient of resistance re-asserts.

TABLE I. Details of the samples investigated. N_A is the acceptor doping density. The width refers to that of the metal layer, the length, and thickness of which in all cases are 160 μm and $\sim$10 nm, respectively.

Sample No.	Metal	Width (μm)	N_A (10^{15}/cm^3)	T_C (K)	ΔT (K)	ΔR_D (Ω)	$\Delta R_D/\Delta T$ (Ω/K)
S1	Pd	16	4.0	310	215	5374	25
S2		32		310	158	892	5.6
S3		64		299	139	333	2.3
S4	Pt	32	1.5	185	69	103	1.5
S5		64		188	64	68	1.06

At any temperature T, the probability of thermionic emission across a barrier of height ϕ_B is $\sim$exp($-\phi_B/kT$), where k is the Boltzmann constant; alternatively, one can think in terms of a SB resistance that is inversely proportional to the excitation probability. Applying this terminology to the NTR region, the excitation probability (SB resistance) increases (decreases) with temperature until it becomes sufficiently large (small) for it to have no effect on the overall resistance of the device at T_2. In the region of $T \sim T_C$, the effective SB resistance is comparable to that of the semiconductor. Importantly, T_C and ΔT are not only decided by the relative values of the semiconductor and metal resistances but crucially by the SB height ϕ_B. If, at a given temperature, the resistances of the metal and semiconductor are comparable, and the measured resistance is a combination of transport through the metal and semiconductor determined by the exact value of ϕ_B. Any change to ϕ_B is thus directly and sensitively reflected in the four-probe device resistance. In all cases in Figures 2 and 3, electrical transport for $T > T_2$ is dominated by conduction through the semiconductor substrate. This is achieved by having a highly resistive metal electrode, ensured by less than 10 nm thickness of the metal film. If the metal is substantially thicker than 10 nm, its resistance is much smaller than the Si substrate at all temperatures, and the conduction is dominated by the metal at all temperatures; consequently, no transition is observed in the R_D-T plot.

We now lay out the background for developing this conceptual framework into a quantitative model (Sec. IV), noting that the experimental data, coupled with theoretical modelling, could offer a single-step technique for characterising the various device parameters, namely, the residual resistivity and temperature coefficient of resistance of the metal film, the semiconductor doping density, and the SB height, along with its temperature dependence. Traditionally, values for the semiconductor- and barrier-related parameters are obtained from a series of I–V measurements across the SB, carried out at various temperatures. At this stage, to create a bridge to the conventional I-V-T approach, it is useful to proceed by referring to a set of such measurements and to use the device parameters generated thereby to inform the model developed to describe the R_D-T data of Figures 2 and 3. The temperature dependent I-V characteristics (measured across the SB) of these devices were recorded in the temperature range of 50–350 K (Figures S1 and S2 in supplementary material).[50] The forward biased characteristic is well described by the standard thermionic emission diffusion theory,[51] where the total current density, J, across a metal-semiconductor junction is given by

$$J = J_o\left(\exp\left(\frac{qV}{\eta kT}\right) - 1\right)$$ (1)

in which

$$J_o = A^*T^2 \exp\left(-\frac{q\phi_B}{kT}\right),$$ (2)

where A^* is the effective Richardson constant for thermionic emission and η is the diode ideality factor. Here, A^* is defined as $A^* = 4\pi q m^* k^2/h^3$, where m^* is the effective mass. Fitting Eq. (1) to the forward bias I-V characteristics, for $V \gtrsim 3kT$, at various temperatures yields J_o and consequently ϕ_B as a function of temperature, shown in Figure S3 in supplementary material.[50] The effective Richardson constant A^* used for p-type Si in the fits is 79.2 A/cm^2/K^2, corrected for the effective mass as 0.66 m_e.

IV. MODELLING THE DEVICE RESISTANCE, R_D

The resistance of the SB device (R_D) in the configuration of Figure 1(b) can be modelled on the basis that the thin metal film and the semiconductor substrate can be considered as a series of resistor elements (r_M and r_S, respectively) in parallel, with the SB (of resistance R_{SB}) incorporated as interconnecting resistors forming an infinite resistor ladder network as shown in Figure 4. To measure the total resistance a known current is sourced and drained through terminals A and B, respectively, and the potential developed in between is measured to compute the device resistance R_D.

Here, the ladder network consists of N cells with all cells identical except the first and last; in each cell, $r_M = R_M/N$ and $r_S = R_S/N$. Although all the SB resistances are denoted by R_{SB} in practice, they may be different due to a spatial distribution of the SB height, ϕ_B, making it is impossible to obtain an exact solution of the equivalent resistance, for large N.

For the metal electrode, a linear fit to the experimental R_D-T data for $T \ll T_C$ generates the best fit values for R_M, with

$$r_M = R_M/N = (R_o + \alpha T)/N.$$ (3)

This linear fit is used to represent the metal resistance and is extrapolated over the entire temperature range investigated.

For the semiconductor, the resistivity is given by
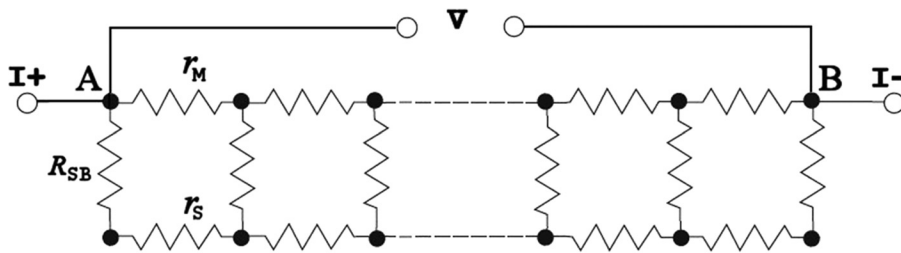
$$\rho_S = \frac{1}{e(\mu_h p + \mu_e n)},$$ (4)

FIG. 4. Schematic of equivalent electrical circuit of Schottky barrier structures used to calculate diode dc resistance, R_D. R_{SB} refers to the barrier resistance, while r_M and r_S refer to metal and semiconductor resistance elements, respectively.

where μ_h is the hole mobility, p is the hole density, μ_e is the electron mobility, and n is the electron density. Depending on the nature of doping (p- or n-type) of the substrate, we retain only the majority carrier term for calculation; here, this is $\mu_h p$. To evaluate R_S as a function of T from Eq. (4), expressions for the carrier density and mobility must be considered. Details of the calculation of the carrier density are well documented in standard semiconductor literature;[51] for a p-type substrate, the primary factors determining the carrier density are the ionized acceptor impurity concentration, N_A^-, and the thermally generated electron density in the conduction band, n. The relevant expression is

$$p = N_A^- + n = N_A \left[1 + g_A \exp\left(\frac{E_A - E_F}{kT}\right)\right]^{-1}$$
$$+ N_C \exp\left(-\frac{E_C - E_F}{kT}\right), \tag{5}$$

where the previously undefined quantities are the ground state degeneracy factor for acceptor levels, g_A (=4 for Si), the acceptor energy level, E_A (=0.045 eV for B-doped Si), the Fermi level E_F, the conduction band energy level, E_C, and the effective densities of states in the acceptor and conduction bands, N_A and N_C, respectively. In determining the mobility of the holes, μ_h (in the case of p-type Si) measurements have shown that this quantity varies with temperature and N_A. Theoretical predictions indicate that μ_h is affected both by lattice vibrations and ionized impurities. For lattice scattering $\mu_h \propto T^{-\gamma}$, where γ is the temperature exponent, taking on a value of $\sim 3/2$ when involving longitudinal acoustical modes. In the case of ionized impurities, around 300 K, the mobility decreases with increasing N_A. The measured mobility at room temperature, $\mu_{h(300K)}$, with an impurity concentration of $\sim 10^{15}$ cm^{-3} is ~ 490 cm^2/V s for p-Si. For low dopant concentrations, mobility decreases with temperature. In practice, experimental results demonstrate a range of values, $1.6 \le \gamma \le 2.8$,[52,53] the larger magnitude originating from additional scattering mechanisms such as non-isotropic effective masses, transverse acoustic phonons, and optical phonons. Overall, the temperature dependence of μ_h may be expressed as

$$\mu_h(T) \approx \mu_{h(300K)} \left(\frac{300}{T}\right)^\gamma. \tag{6}$$

Thus, having determined the carrier density and mobility along with their temperature dependence, a complete expression may be obtained for R_S and consequently r_S.

Finally, turning attention to the SB resistance, a mathematical expression to model R_{SB} and its temperature

dependence can be given on the basis of Eqs. (1) and (2). Under the present measurement conditions, no bias is explicitly applied across the barrier and with a maximum potential drop ~ 10 mV along the length of the device (i.e., across terminals AB) the effective bias across the Schottky barrier is extremely small and is actually a function of position, depending on the exact path of transport through the device. We thus assume that the dominant carrier transport mechanism across the barrier at any point is primarily governed by Eq. (1), with quasi-zero applied bias, and that the barrier resistance is thus given by

$$R_{SB} \propto \frac{1}{J_0} = \frac{1}{A^* T^2 \exp\left(-\dfrac{q\phi_B}{kT}\right)} \tag{7}$$

under both infinitesimal forward and reverse bias conditions. Assuming the effective bias across the barrier, at any point along the elongated metal electrode is of the order of a few mV or less the symmetric use of this expression is reasonable. This is certainly more so the case at lower temperatures in the region of T_C, where the form of the decrease in R_{SB} will be most sensitively manifest in the overall device response. If the bias-symmetric application of Eq. (7) at higher temperatures is less appropriate, it is of much less consequence since R_{SB} has effectively collapsed by that stage—the metal and semiconductor are then effectively in intimate electrical contact and R_D is dominated by the component resistances R_M and R_S. It is important to note that the SB height is reported in literature to be a linear function of temperature, a behavior ascribed to barrier inhomogeneities[54,55] of the junction. The SB heights calculated from the I-V-T characteristics of the devices studied here also show a linear T dependence[50] of the form

$$\phi_B = \phi_{300K}(1 + \beta(T - 300)) \tag{8}$$

with $\beta \sim 0.25$ meV/K and a device dependent ϕ_{300K}. Consequently, we have also incorporated a temperature dependent $\phi_B(T)$, as described by Eq. (8), with ϕ_{300K} and β as fit parameters in modelling the device resistance R_D. However, the actual fitting of the data in Figures 2 and 3 is done independently of any input from the I-V-T approach; differences in the value of ϕ_B generated from analysis of I-V-T and R_D-T data are tabulated in Table S1[50] of supplementary material and discussed briefly later.

Having derived expressions for r_M, r_S, and R_{SB}, we are now in a position to calculate the effective resistance between A and B. Analytical calculation of the overall resistance for $N > 1$ becomes very cumbersome; thus, it was

evaluated numerically by a custom written computer code implemented using Matlab©. For the fits shown in Figures 2 and 3, a 10-cell configuration was used to model the data. In general, a multi-cell calculation is required to replicate the experimental data well in the vicinity of the turning points at T_1 and T_2 on the R_D-T curve. The parameters derived from the 10-cell calculation of the modelled data of Figures 2 and 3 are given in Table II. The data, which are physically based, are highly consistent across the sample range.

To further elucidate the analysis in a manner that offers direct physical insight, the $N = 1$ case is considered; for this case, the effective diode resistance may be expressed analytically as

$$\frac{1}{R_D} = \frac{1}{R_{AB}} = \frac{1}{R_M} + \frac{1}{(R_{SB} + R_S)}$$
$$= \frac{1}{(R_o + \alpha T)} + \left(\frac{1}{A^* T^2 \exp(-q\phi_B/kT)} + \frac{g}{(ep\mu_h)} \right)^{-1},$$
(9)

where g is a geometric factor given by L/A_S, A_S being the area of the semiconductor cross-section[56] and L is the metal electrode length. Interestingly, no scaling factors are required for either of the last two terms in Eq. (9). Figure 5 shows the component parts of the model for the $N = 1$ case and their combination to yield the device R_D-T curve. For purposes of illustration, this is done using the data of S5 as an example since all resistances can be plotted comfortably on the same scale to show all the salient features and since the N = 1 fit is of good quality in this case. The linear temperature dependence of R_M (Eq. (3)) is characterized at low temperature but is extrapolated to higher temperature, as indicated by the dashed line.

In relation to the semiconductor curve, R_S, there is a run-off to very high resistance at low temperature as the carriers get "frozen out." This feature is not seen in the experimental data because the current flow in this temperature range is solely via the metal electrode. If the barrier height were significantly lower, then the R_D-T characteristic would reflect this phenomenon, provided still that the metal electrode had significant resistance. (It might also be remarked that, relative to a pure semiconductor thermistor, the presence of the metal electrode, allied with measurement along the length of the electrode, ensures tractable, easily
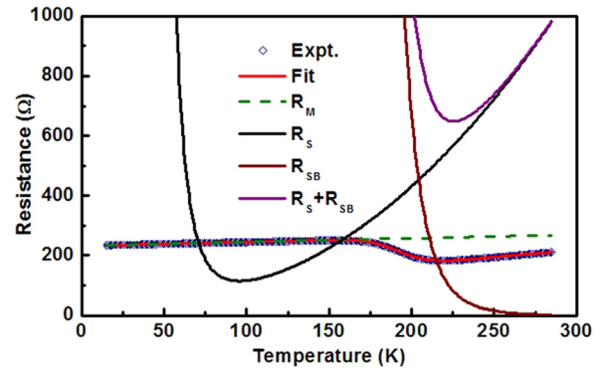

FIG. 5. Experimental and fitted model data for sample S5 (Pd/p-Si) showing the constituent resistance elements, comprising the metal electrode resistance, R_M, semiconductor resistance, R_S, and effective resistance associated with the Schottky barrier, R_{SB}.

measurable device operation over the entire temperature range.) In the high-T regime, R_S exhibits a positive curvature, characteristic of semiconductor transport. This too can be manifested in R_D depending on the relative contribution of metal and semiconductor in this regime. The next step in the development of Figure 5 is curve R_{S+SB} representing the combined effective resistance of barrier and semiconductor. The main point to note is that the region of falling resistance in R_{S+SB} (with increasing temperature) is clearly the origin of the drop seen in R_D as this is quite distinctly removed (by >100 K) from the resistance drop in R_S due to thermal excitation of carriers within the semiconductor. Finally, the combination of R_M and R_{S+SB} yields the overall device resistance according to Eq. (9).

The above analysis is based entirely on the standard thermionic emission diffusion theory in the quasi-zero bias limit, applied to the SB within the 10-cell resistor network model of Figure 4. Beyond the obvious point of evidential justification for the above approach, namely, that it works very well as shown by Figures 2, 3, and 5 (for the single-cell case), we comment on two further points in relation to the physical basis of the model. First, it is re-iterated that the quasi-zero bias condition allows us to treat the SB as a simple resistive element for all samples and across the entire temperature range. Second, the SB height obtained from the model R_D-T plots (Table II) is systematically lower than those obtained from analysis of the I-V-T plots, as shown in Figure S3 and Table S1 in supplementary material.[50] This is likely due to the lateral transport geometry underpinning the R_D-T data and the contrast in the bias conditions pertaining to the SB, under which the barrier height is calculated, in the two methodologies. For the R_D-T measurements, no bias is explicitly applied to the semiconductor and only a small (quasi-zero) bias appears across the SB, which accentuates contributions from the lower SB height regions of the junction. In contrast, necessarily the high bias regime of the I-V-T data is used to calculate the SB height. Carriers moving across the SB evidence different *effective* SB heights, at quasi-zero and for large bias regimes,[36,37] as probed by the two techniques. Nonetheless, we reiterate that the data of Table II are very consistent across the sample range

TABLE II. Values of the best-fit parameters as defined in the text for samples S1–S5.

Sample / Parameters	S1	S2	S3	S4	S5
N_A (10^{15} cm^{-3})	5.2	4.22	4.05	1.02	1.02
γ	2.1	2.3	2.8	2.29	2.35
μ (cm^2/Vs)	426	455	443	500	495
R_0 (Ω)	6247	1334	544	324	232
α (mΩ K^{-1})	213	375	197	92	127
$\phi_{B(T=300 K)}$ (meV)	380	381	338	288	287
β (meV/K)	0.217	0.193	0.237	0.110	0.140

(especially for the pair of Pt/p-Si samples) are physically based and realistic, and underpin the excellent fits of calculated to experimental data.

V. OUTLINING THE APPLICATION POTENTIAL OF THE ALTERNATIVE METHODOLOGY

In order to further elucidate the advantages of the presented methodology and potential for future applications, we refer to the simulated R_D-T of an idealized device shown in Figure 6(a) (solid black line). The metal electrode is designed to have device (metal) resistance $R_D \sim 5\,k\Omega$ at low T, while the high-T resistance is a few hundred Ohms. Other device parameters are chosen to be typical of those given in Table II for devices S4 and S5 with $\varphi_B = 300\,meV$ at 150 K. The sharpness of the transition centered around 150 K is quantified here by calculating the differential dR_D/dT (inset of Figure 6(a)). The full width at half maximum shows $\delta T \sim 20\,K$. As observed, the metal and semiconductor properties determine the sharpness of transition while the T_C is primarily determined by the SB height. The family of curves in Figure 6(a) is generated by decreasing the SB height from 300 to 200 meV in steps of 25 meV with the other parameters unchanged; the arrow indicates decreasing barrier height. Consequently, T_C shifts to lower temperatures with marginal increase in the sharpness of transition. Alternatively, when
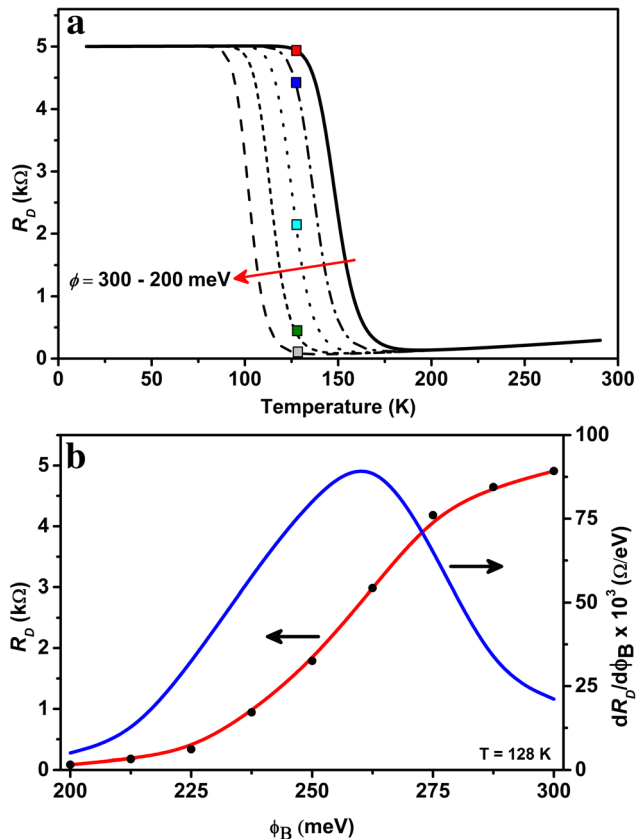
observed at a fixed temperature R_D decreases with decreasing SB height; Figure 6(b) (left axis) plots this change in R_D at $T = 128\,K$, as the SB height collapses. The points in Figure 6(a) at which R_D is sampled are denoted by squares. The derivative ($dR_D/d\varphi_B$) plotted in Figure 6(b) (right axis) shows a high sensitivity of $\sim 10^5\,\Omega/eV$ at its peak, located around the T_C of the corresponding R_D-T plot. Though the sensitivity of R_D is apparently a function of SB height, it is really decided by the location of the measurement point within the transition region in the corresponding R_D-T curve. Notably, over the entire transition region the sensitivity is always higher than $10^4\,\Omega/eV$.

Therefore, with the operating temperature located within the transition region (it is generally desirable that this region is just above ambient temperature), R_D becomes an excellent "sniffer" of small changes in SB height and in turn any external parameter that might induce such change. Thus, based on the above property, the authors have demonstrated a highly sensitive (1 ppm) hydrogen detector[31] using the device configuration of Figure 1; indeed, with the value of R_{max} not being optimally located in temperature in that study, there is ample scope for improved performance and further lowering of the detection threshold. To re-iterate a key finding of that study, the sensitivity of R_D to hydrogen concentration, C_H, was significant for very low concentrations ($C_H < 20\,ppm$), since R_D effectively probes the (inverse of) junction conductance, which changes significantly in the near-zero junction bias regime. By contrast, the hydrogen detection sensitivity of Schottky diodes operated in the conventional I-V measurement mode is extremely low for $C_H < 20\,ppm$, but increases rapidly in the range of $10^2 < C_H < 10^4$ before losing sensitivity for very high C_H (refer Feng *et al.*[31] and references therein). It is worth mentioning that in addition to the primary effect of interfacial atomic hydrogen altering the SB height, there is also a possible effect on the semiconductor resistance due to hydrogen passivation of the dopants, which may also, in turn, affect the barrier profile.[57] However, any such secondary effects are not explicit in our present analysis.

Comparable sensitivity has also been reported for similar Pt-InN devices;[58] however, while those macroscopic scale ($0.5 \times 2.5\,mm$) devices appear to share the same operating principle as our devices, the mechanism of current flow is not elucidated or analyzed in that work. On the basis of the model discussed above, we conclude that the high sensitivity of R_D to the SB height stems from exponential interdependence between R_D and the SB height (refer Eqs. (7) and (9)), a feature guaranteed by an important aspect of this measurement technique, namely, negligible (quasi zero) voltage drop across the Schottky junction. The exponential interdependence and thereby sensitivity is progressively muted with increasing voltage drop across the junction. The developed model not only enhances our understanding of the high sensitivity reported by Feng *et al.*[31] and Chang *et al.*[58] but crucially helps in optimization of the device parameter space for improved performance. We additionally note that the use of a high-resistance metal electrode in the active device region, inherent in the structure of this type of Schottky device, brings with it the corollary of facilitating better molecular

FIG. 6. (a) Simulated R_D-T plots of a Schottky diode device with the barrier height changed from 300 to 200 meV in steps of 25 meV; arrow indicates decreasing barrier height. Inset shows the dR_D/dT plot of the device with 300 meV barrier height. (b) Plot of R_D with the decreasing barrier height (obtained from (a)) at a constant temperature $T = 128\,K$ and variation of $dR_D/d\varphi$ with barrier height at same temperature.

access to the SB region through a very thin, highly porous metal electrode structure.

It is re-iterated that the methodology described above is of general applicability to all metal-semiconductor combinations that form Schottky contacts, provided the "metal" electrode can controllably be made very thin or resistive. In addition to very thin, but otherwise "standard" metal film electrodes such as are used here and in Refs. 48 and 58, the methodology could be readily extended to include, e.g., the nanoparticle-Pd/diodes reported by Chou *et al.*,[29] the various carbon-based Schottky contacts such as the semi-metal/semiconductor, graphite/-Si (or/-GaAs or /4 H-SiC) structures of Tongay *et al.*[38] and single or double layer graphene electrodes.[39–44] Also, there is an interesting class of 1D ZnS nanorod/carbon nanotube coaxial Schottky junctions,[59] which would be readily amenable to the methodology reported here.

Finally, the methodology we report is optimally realized through the formation of high-aspect-ratio Schottky diodes, a configuration which is highly amenable to exploitation in the context of semiconducting nanowire structures. Of particular interest and relevance, we note the formation of Schottky-contact devices based on single semiconductor nanowires of Ge,[60] ZnO,[61] and GaAs,[62] all with photodetection as the targeted application. Such single semiconductor structures with a very thin, resistive metal adlayer forming a Schottky contact (and suitably contacted for 4-point probe measurement) would offer an extended arena with some interesting physical contrasts for the proposed methodology. The reason for physical contrast with the devices presented here is that when the semiconductor itself is nano-dimensioned, the physics of the depletion region and conduction across the Schottky barrier is significantly modified,[63] with the key modification being an enhanced tunnelling regime. Such effects have been explicitly taken into account in an investigation of hydrogen detection using a GaN/Pt Schottky honeycomb network.[64]

VI. CONCLUSION

In this work, a different perspective on Schottky diode fabrication and measurement has been taken to yield R_D-T characteristics that are sensitive to all of the metal, SB, and semiconductor properties. The key feature of the R_D-T curves is a region of NTR ($dR_D/dT < 0$) centered at a temperature T_C, which is primarily decided by the SB height. The magnitude of the NTR though is shown to be critically dependent on the resistance of the metal electrode relative to that of the underlying semiconductor. The R_D-T behavior is effectively and precisely described using a simple-in-principle resistor network model, which further elucidates how one might control the characteristics of the R_D-T curve (T_C, ΔR, ΔT, and to some extent $\Delta R/\Delta T$) or, alternatively, how such curves could be used for characterization analysis that is complementary to that based on conventional I-V-T and C-V measurements. Notably, within the NTR region, the device resistance is shown to be highly sensitive to the SB height due to their exponential interdependence; a feature that can be effectively exploited to perform molecular sensing of species that accumulate at the Schottky interface leading to a change in barrier height. We can confirm that this is indeed the case by using resistive-Pd/n-InP diodes in the above discussed 4-probe configuration to detect hydrogen to the ppm level,[31] displaying greater sensitivity at low concentration levels than the same devices operated with the standard contact configuration directly across the SB. More obviously, the device can be used as a limited range (but selectable) temperature sensor and also as a thermally controlled switch with definite cut-off resistances beyond specific temperatures. Since the ΔR between the high and low resistance states can be as large as $\sim 10^3$, the device resistance can change by that amount once it crosses pre-specified temperatures (ΔT around T_C). Thus, both trigger and control of a temperature dependent parameter of a system can also be achieved by employing this incarnation of the Schottky junction.

[1]W. Schottky, Naturwissenschaften **26**(52), 843–843 (1938).
[2]N. F. Mott, Math. Proc. Cambridge Philos. Soc. **34**, 568 (1938).
[3]H. A. Bethe, MIT Radiation Laboratory Report No. 43, 1942, p. 12.
[4]A. Maestrini, J. Ward, G. Chattopadhyay, E. Schlecht, and I. Mehdi, Frequenz **62**(5–6), 118–122 (2008).
[5]F. Sizov, Opto-Electron. Rev. **18**(1), 10–36 (2010).
[6]H. T. Chen, W. J. Padilla, J. M. O. Zide, A. C. Gossard, A. J. Taylor, and R. D. Averitt, Nature **444**(7119), 597–600 (2006).
[7]L. E. Calvet, R. G. Wheeler, and M. A. Reed, Appl. Phys. Lett. **80**(10), 1761–1763 (2002).
[8]J. M. Larson and J. P. Snyder, IEEE Trans. Electron Devices **53**(5), 1048–1058 (2006).
[9]R. J. Moon, M. I. Jeong, S. V. Chandra, K. H. Shim, M. Jang, H. B. Hong, S. Y. Chang, and C. J. Choi, J. Electrochem. Soc. **156**(8), H621–H624 (2009).
[10]R. Singh, J. A. Cooper, M. R. Melloch, T. P. Chow, and J. W. Palmour, IEEE Trans. Electron Devices **49**(4), 665–672 (2002).
[11]T. Hashizume, J. Kotani, and H. Hasegawa, Appl. Phys. Lett. **84**(24), 4884–4886 (2004).
[12]M. W. Allen, X. J. Weng, J. M. Redwing, K. Sarpatwari, S. E. Mohney, H. von Wenckstern, M. Grundmann, and S. M. Durbin, IEEE Trans. Electron Devices **56**(9), 2160–2164 (2009).
[13]S. Vempati, S. Chirakkara, J. Mitra, P. Dawson, K. K. Nanda, and S. B. Krupanidhi, Appl. Phys. Lett. **100**(16), 162104 (2012).
[14]S. W. Kim, K. Ogata, K. Maejima, S. Fujita, and S. Fujita, *Compound Semiconductors 2001* (CRC Press, 2002), pp. 671–675.
[15]W. I. Park, G.-C. Yi, J.-W. Kim, and S.-M. Park, Appl. Phys. Lett. **82**(24), 4358–4360 (2003).
[16]T. Strupeit, C. Klinke, A. Kornowski, and H. Weller, ACS Nano **3**(3), 668–672 (2009).
[17]P. Bondavalli, L. Gorintin, G. Feugnet, G. Lehoucq, and D. Pribat, Sens. Actuators, B **202**, 1290–1297 (2014).
[18]K.-H. Kim, D. Brunel, A. Gohier, L. Sacco, M. Châtelet, and C.-S. Cojocaru, Adv. Mater. **26**(25), 4363–4369 (2014).
[19]H. Cetin and E. Ayyildiz, Phys. B: Condens. Matter **394**(1), 93–99 (2007).
[20]V. I. Shashkin, A. V. Murel, V. M. Daniltsev, and O. I. Khrykin, Semiconductors **36**(5), 505–510 (2002).
[21]H. I. Chen and Y. I. Chou, Semicond. Sci. Technol. **18**(2), 104–110 (2003).
[22]D. R. T. Zahn, S. Park, and T. U. Kampen, Vacuum **67**(1), 101–113 (2002).

[23]H. Haick, M. Ambrico, T. Ligonzo, R. T. Tung, and D. Cahen, J. Am. Chem. Soc. **128**(21), 6854–6869 (2006).

[24]Z. Zhang, Z. J. Qiu, R. Liu, M. Ostling, and S. L. Zhang, IEEE Electron Device Lett. **28**(7), 565–568 (2007).

[25]A. Salehi and A. Nikfarjam, Sens. Actuators, B **101**(3), 394–400 (2004).

[26]S. J. Pearton, F. Ren, Y. L. Wang, B. H. Chu, K. H. Chen, C. Y. Chang, W. Lim, J. S. Lin, and D. P. Norton, Prog. Mater. Sci. **55**(1), 1–59 (2010).

[27]W. P. Kang and Y. Gurbuz, J. Appl. Phys. **75**(12), 8175–8181 (1994).

[28]J. Schalwig, G. Muller, U. Karrer, M. Eickhoff, O. Ambacher, M. Stutzmann, L. Gorgens, and G. Dollinger, Appl. Phys. Lett. **80**(7), 1222–1224 (2002).

[29]Y. I. Chou, C. M. Chen, W. C. Liu, and H. I. Chen, IEEE Electron Device Lett. **26**(2), 62–65 (2005).

[30]J. T. Yan and C. T. Lee, Sens. Actuators, B **143**(1), 192–197 (2009).

[31]L. Feng, J. Mitra, P. Dawson, and G. Hill, J. Phys.: Condens. Matter **23**(42), 422201 (2011).

[32]J. H. Werner and H. H. Guttler, J. Appl. Phys. **69**(3), 1522–1533 (1991).

[33]P. G. McCafferty, A. Sellai, P. Dawson, and H. Elabd, Solid-State Electron. **39**(4), 583–592 (1996).

[34]R. T. Tung, Mater. Sci. Eng. R **35**(1–3), 1–138 (2001).

[35]S. Chand and S. Bala, Appl. Surf. Sci. **252**(2), 358–363 (2005).

[36]R. T. Tung, Phys. Rev. B **45**(23), 13509–13523 (1992).

[37]R. T. Tung, Appl. Phys. Rev. **1**(1), 011304 (2014).

[38]S. Tongay, T. Schumann, and A. F. Hebard, Appl. Phys. Lett. **95**(22), 222103 (2009).

[39]Y. An, A. Behnam, E. Pop, and A. Ural, Appl. Phys. Lett. **102**(1), 013110 (2013).

[40]C.-C. Chen, M. Aykol, C.-C. Chang, A. F. J. Levi, and S. B. Cronin, Nano Lett. **11**(5), 1863–1867 (2011).

[41]G. Fan, H. Zhu, K. Wang, J. Wei, X. Li, Q. Shu, N. Guo, and D. Wu, ACS Appl. Mater. Interfaces **3**(3), 721–725 (2011).

[42]X. Li, H. Zhu, K. Wang, A. Cao, J. Wei, C. Li, Y. Jia, Z. Li, X. Li, and D. Wu, Adv. Mater. **22**(25), 2743–2748 (2010).

[43]B. Nie, J.-G. Hu, L.-B. Luo, C. Xie, L.-H. Zeng, P. Lv, F.-Z. Li, J.-S. Jie, M. Feng, C.-Y. Wu, Y.-Q. Yu, and S.-H. Yu, Small **9**(17), 2872–2879 (2013).

[44]S. Sonde, F. Giannazzo, V. Raineri, R. Yakimova, J. R. Huntzinger, A. Tiberj, and J. Camassel, Phys. Rev. B **80**(24), 241406 (2009).

[45]P. Dawson, L. Feng, L. Penate-Quesada, J. Mitra, and G. Hill, J. Phys. D: Appl. Phys. **44**(12) 125101 (2011).

[46]J. E. Murguia, J. M. Mooney, and W. S. Ewing, Opt. Eng. **29**(7), 786–794 (1990).

[47]P. R. Norton, Opt. Eng. **30**(11), 1649–1663 (1991).

[48]K. Oto, S. Takaoka, K. Murase, and S. Ishida, J. Appl. Phys. **76**(9), 5339–5342 (1994).

[49]D. Kojima, K. Makihara, J. Shi, and M. Hashimoto, Appl. Surf. Sci. **169**, 320–324 (2001).

[50]See supplementary material at http://dx.doi.org/10.1063/1.4922974 for experimental I-V-T data and temperature dependent Schottky barrier heights obtained from their fits.

[51]S. M. Sze and K. K. Ng, *Physics of Semiconductor Devices*, 3rd ed. (John Wiley and Sons, Inc., Hoboken, New Jersey, 2007).

[52]M. S. Tyagi, *Introduction to Semiconductor Materials and Devices* (John Wiley and Sons, 1991).

[53]C. Jacoboni, C. Canali, G. Ottaviani, and A. A. Quaranta, Solid-State Electron. **20**(2), 77–89 (1977).

[54]A. A. Kumar, V. Janardhanam, V. R. Reddy, and P. N. Reddy, Superlatt. Microstruct. **45**(1), 22–32 (2009).

[55]M. B. Reddy, A. A. Kumar, V. Janardhanam, V. R. Reddy, and P. N. Reddy, Curr. Appl. Phys. **9**(5), 972–977 (2009).

[56]A_S is calculated as the product of the width of the metal and the thickness of the semiconductor.

[57]R. L. Van Meirhaeghe, W. H. Laflere, and F. Cardon, J. Appl. Phys. **76**, 403 (1994).

[58]C. Yuh-Hwa, C. Kai-Kuen, G. Shangjr, and J. A. Yeh, Appl. Phys. Express **3**(11), 114101 (2010).

[59]D. Wei, Y. Liu, L. Cao, H. Zhang, L. Huang, and G. Yu, Chem. Mater. **22**(2), 288–293 (2010).

[60]C.-J. Kim, H.-S. Lee, Y.-J. Cho, K. Kang, and M.-H. Jo, Nano Lett. **10**(6), 2043–2048 (2010).

[61]K. ul Hasan, N. H. Alvi, J. Lu, O. Nur, and M. Willander, Nanoscale Res. Lett. **6**(1), 348 (2011).

[62]H. Wang, Appl. Phys. Lett. **103**(9), 093101 (2013).

[63]G. D. J. Smit, S. Rogge, and T. M. Klapwijk, Appl. Phys. Lett. **81**(20), 3852–3854 (2002).

[64]A. Zhong, T. Sasaki, and K. Hane, Int. J. Hydrogen Energy **39**(16), 8564–8575 (2014).